Clay Minerals, (2018) **53**, 675–690

Clay minerals related to the late magmatic activity of the Piton des Neiges (Réunion Island): consequence for the primitive crusts

GILLES BERGER[1], DANIEL BEAUFORT[2] AND RAPHAËL ANTOINE[1,3,*]

[1] *IRAP, CNRS, UPS, Observatoire Midi-Pyrénées, 14 Av. E. Belin, 31400 Toulouse, France*
[2] *IC2MP, Université Poitiers, 40 Av. Recteur Pineau, 86022 Poitiers Cedex, France*
[3] *CEREMA Normandie-Centre, 76121 Le Grand Quevilly, France*

(*Received 22 March 2018; revised 24 June 2018; Accepted Manuscript published online: 17 December 2018; Version of Record published online: 23 January 2019; Associate Editor: M. Buatier*)

ABSTRACT: This paper describes a detailed petrographic and isotopic study of hypabyssal sheets of quartz-syenite that represent the ultimate differentiation product of the oceanite alkaline magmatic reservoir of the Piton des Neiges stratovolcano (Réunion Island). Clay minerals of the corrensite to chlorite series crystallized during the late-magmatic activity, with quartz, carbonates and accessory minerals from juvenile fluids filling the primary porosity of the quartz-syenite. It is proposed that a double chemical transfer occurred at the end of the crystallization process: degassing of the exsolved CO_2-rich and SiO_2-rich fluid from the magmatic chamber through the porous quartz-syenite and diffusion of Al, Fe and Mg from the intruded basalts affected by the juvenile fluids towards the primary porosity of the quartz-syenite, feeding the crystallization of late-magmatic clays in the residual primary pores after quartz and carbonate deposition. This process may be generalized to alkaline plutonism, as well as to the primitive crusts of terrestrial planets, and may be the first source of clays in early planets.

KEYWORDS: clay minerals, alkali magmatism, quartz-syenite, oceanite, Mars.

The physicochemical processes associated with heat and magma transfer occur at various magmatic stages from partial melting, to storage, to volcanic eruption. Among them, subsolidus reactions such as feldspar perthitization have been identified as causes of redistribution of primary porosity (diktytaxitic voids) to secondary porosity of the felsic minerals. A typical example has been documented in the granite of Kakkonda geothermal field, Japan, where deep drilling allowed sampling of granite at high temperatures just after solidification of magma (Sasaki *et al.*, 2003).

Associated with the final stage of crystallization is the concentration and exsolution of aqueous-rich volatiles. Hydrous magmas are very common in the most differentiated calc-alkaline magmatic series, where the presence of micas and amphiboles and associated mesothermal alteration testify to the importance of juvenile fluids. Recent studies have suggested that clay minerals may form during the last magmatic stage or immediately after the crystallization of basalts (Meunier *et al.,* 2008, 2012; Berger *et al.*, 2014). This idea that authigenic clay minerals may be the ultimate hydrous manifestation of the differentiation process in magmatic rocks contradicts the assumption that clay minerals in natural systems are uniquely indicative of weathering or hydrothermal alteration. However, these studies did not identify the means by which the elements are transferred to secondary hydrous silicates and their chronology with respect to late-magmatic evolution. In particular, the direct crystallization of Fe,Mg-clays from the last

*E-mail: gilles.berger@irap.omp.eu
https://doi.org/10.1180/clm.2018.51

hydrous melt at the end of differentiation (Meunier *et al.*, 2008) is questionable because it seems inconsistent with the low Fe^{2+} and Mg contents of the silicate melt at the end of magmatic differentiation.

The present study focused on the formation of clay minerals in hypabyssal sheets of intermediate oversaturated alkali rocks that represent the ultimate differentiation products of the oceanite alkaline magmatic reservoir of the Piton des Neiges volcano in Réunion Island, western Indian Ocean, France. The quartz-syenite hypabyssal sheets represent the most alkaline differentiated terms of a cone sheet complex previously described by Upton & Wadsworth (1967). These intrusive rocks are suitable candidates for investigating the late stage of crystallization in the shallow reservoir of oceanite magma and the related exsolution of volatiles. This is because the terminal explosive activity of the volcano froze the textural and mineralogical properties of these intrusive rocks at a post-magmatic stage that is generally not accessible to direct observation. In this study, emphasis is put on ferromagnesian hydrous phyllosilicates that draw our attention to a possible late-magmatic origin. Petrographic descriptions with optical and electron microscopy and isotopic analyses of silica and carbonate phases that coexist with the phyllosilicates were used to provide arguments on the origin and evolution of the fluids in a general self-consistent scheme.

The differentiation of oceanite magmas producing alkaline and hydrous products, even if anecdotal today when compared to the large amounts of continental rhyolites occurring at the surface of the Earth, may have been much more significant in the early Earth, for which the hydration conditions of the primitive crust are still under debate (Ohtani, 2005). This question may also be expanded to the general case of the telluric planets, particularly those that did not undergo plate tectonics: the recent observations of mugearite-type basalts in the Gale Crater on Mars by the *Curiosity* Rover of the Mars Science Laboratory mission (Stolper *et al.*, 2013; Sautter *et al.*, 2014, 2015) illustrate that it is important to identify the last term of the alkaline series and the associated post-magmatic phyllosilicates because they may constitute alternative sources of clays in dry climates (an ongoing issue for Mars; see *e.g.* Cannon *et al.*, 2017).

REGIONAL SETTING

The island of Réunion is a large alkaline volcanic complex located in the western Indian Ocean (Fig. 1). It is composed of two major volcanoes: the highly

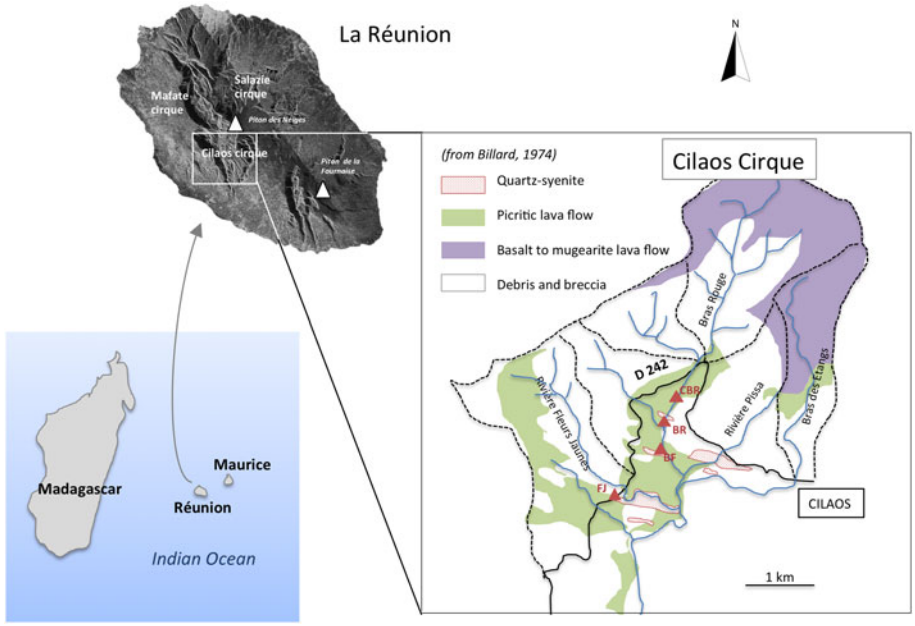

FIG. 1. Locations of the sampling sites. CBR = Bras Rouge waterfall (RUN 1, RUN 2); BR = Bras Rouge (RUN 3, RUN 8, BRA 4); FJ = batholith at Fleur Jaune (RUN 13, RUN 14, BACH 1); BF = Bassin Fouquet (RUN 11).

https://doi.org/10.1180/clm.2018.51 Published online by Cambridge University Press

active Piton de la Fournaise that erupts picritic basalts and the Piton des Neiges – now inactive – that was built from a more differentiated magmatic complex. The Piton des Neiges consists of a large stratovolcano that has been dissected by erosion in its central part, exposing more than 1500 m of a lower unit of lava flow and pyroclastic breccia (oceanite series), overlaid by a younger differentiated series consisting of more alkaline lavas, pyroclastic rocks and intrusive rocks (Upton & Wadsworth, 1965). The volcanic rocks of the oceanic series underwent severe hydrothermal alteration with extensive zeolitization prior to the extrusion of the differentiated series (Rançon, 1985). The terminal phase of the differentiated volcanic series (dated at *ca.* 12,000 years) is marked by emplacement of cone-sheet hypabyssal quartz-syenite through the underlying oceanite formation in a context of large explosive dynamism. Numerous hypabyssal sheets ranging in thickness from a few centimetres to >100 m are emplaced within a roughly circular area of 10 km radius from the estimated position of the main volcanic vent (Upton & Wadsworth, 1965, 1967). The edifice is deeply dissected and the volcanic sequence can be sampled easily in amphitheatre-headed valleys. We focused our attention on the hypabyssal sheets that crop out in the Cilaos Cirque (Fig. 1), representing the declining stage of the Piton des Neiges volcano. The alkaline hypabyssal sheets that intrude into the altered basalts of the lower oceanite series are assumed to be contemporaneous with the lavas of the differentiated series and are sufficiently coarse-grained for the use of the plutonic nomenclature of quartz-syenite. The main volcanic rocks of the Cilaos Cirque (picritic basalt, basalt lava flow, quartz-syenite and volcanic breccia) are mapped in Fig. 1, and some typical outcrops are shown in Fig. 2.

SAMPLES AND ANALYTICAL METHODS

The alkali hypabyssal sheets and the adjacent intruded basaltic rocks have been sampled in various places in the Cilaos Cirque (Fig. 1). Nine rock samples were studied (Table 1). They come from four sites in which quartz-syenite sheets crop out. Five samples were taken from quartz-syenite of various thicknesses, grain sizes and degrees of argilization (RUN 1, RUN 8, RUN 11, RUN 13 and BACH 1). Three other samples were taken from the damaged basaltic rock close to the contact with quartz-syenite. These samples are characterized by brecciation, injection or inclusion of differentiated magmatic materials of syenitic composition (RUN 3, BRA 4 and RUN 14, respectively). Finally, a representative sample of the host basalt was also collected (RUN 2).

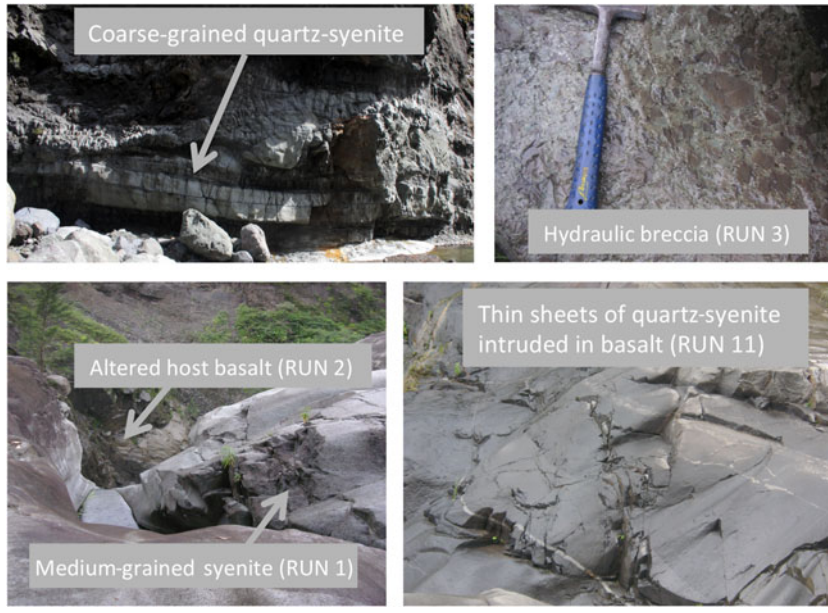

FIG. 2. Outcrops of the studied samples.

https://doi.org/10.1180/clm.2018.51 Published online by Cambridge University Press

Table 1. Locations of samples in this study.

Outcrop	Sample name	Rock description
Bras Rouge waterfall	RUN 1	Medium-grained quartz-syenite (poorly argillized)
	RUN 2	Host basalt (altered)
	RUN 8	Coarse-grained quartz-syenite (moderately argillized)
Bras Rouge Creek	RUN 3	Brecciated contact between the intrusive quartz-syenite and basaltic host rock
	BRA 4	Ocelli of quartz-syenite in basalt (moderately argillized)
	BACH 1	Coarse-grained quartz-syenite (non-argillized)
Fleur Jaune	RUN 13	Fine-grained quartz-syenite (poorly argillized)
	RUN 14	Intrusive patches of quartz-syenite in the host basalt with <1 m of the intrusive contact (moderately argillized)
Bassin Fouquet	RUN 11	Thin sheet (<10 cm) of quartz-syenite (moderately argillized) intruded in basalt

Petrographic studies were performed on both thin sections and rock fragments of each sample using a polarizing optical microscope (Nikon® Eclipse E600POL) and a JEOL 5600 LV scanning electron microscope (SEM) equipped with a Bruker® XFlash 4030 Silicon drift energy-dispersive X-ray (EDX) spectrometer apparatus. The SEM observations were performed in secondary electron imaging mode and/or backscattering electron mode on thin, carbon-coated sections. The analytical conditions for the quantitative chemical analysis of clay minerals by EDX were 15 kV accelerating voltage, 1 nA sample current, a counting time of 60 s and a working distance of 16.5 mm. The standards used for quantitative chemical analysis consisted of albite (Na, Al, Si), almandine (Mg, Fe), diopside (Ca), orthoclase (K) and spessartine (Mn). The matrix corrections were performed using integrated programs (PhiRhoz correction). The reproducibility of the standard analyses was nearly 1.5% for all of the elements, except Na, which attained a reproducibility of 3%.

When clay minerals were identified in the petrographic study, the samples were ground in an agate mortar and dispersed in distilled water by ultrasonic treatment. The <5 μm size fraction was considered as representative of the clay fraction of rocks on the basis of SEM observation of the clay particles. The <5 μm clay fraction was extracted from suspension in distilled water by centrifugation and the clays were analysed in their natural state (no ionic saturation). X-ray diffraction (XRD) analyses were performed using a Bruker D8 XRD diffractometer (Cu-$K\alpha^{1+2}$ radiation) on randomly oriented powders of the bulk samples and on oriented preparations of the clay fraction under air-dried (AD) and ethylene glycol (EG)-saturated conditions. The XRD traces of oriented preparations were acquired in the 2–30° 2θ angular range with 0.02°2θ steps and a counting time of 2 s per step. The XRD patterns of randomly oriented preparations were acquired in the 2–65°2θ angular range with 0.025°2θ steps and a counting time of 2 s per step.

The bulk-rock composition of four selected samples, representing the basaltic and the differentiated terms of the series, was analysed by the Analytical Research Facility that is part of the Centre de Recherches Pétrographiques et Géochimiques (CRPG), Nancy, France. A few grams of crushed sample are fused in $LiBO_2$ then dissolved in 2% HNO_3 before analysis by inductively coupled plasma–optical emission spectrometry (Thermo Fischer ICap 6500).

The isotopic measurements of O and C by secondary ion mass spectrometry (SIMS) were carried out using a CAMECA IMS-1270 instrument (CRPG-CNRS, Nancy) with a focused Cs^+ beam (10 kV, from 4 to 8 nA) with a spatial resolution of 10 μm. The typical acquisition sequences were 25–35 cycles of 2 s duration each. Most of the instrumental conditions are similar to those described by Rollion-Bard *et al.* (2007). The instrumental deviation was corrected by analysing reference material: DPA (ankerite) and BRET 'in-house' standards for carbonate, and QzBresil and NL615 for the siliceous phases.

RESULTS

The petrological characterization of the samples carried out at microscopic scale gave information on the crystallization sequence of the pore-filling phases in the quartz-syenite rocks. The results are presented according to rock facies or mineral type. Finally, the isotopic analyses performed on selected samples according to the petrographic data are shown.

https://doi.org/10.1180/clm.2018.51 Published online by Cambridge University Press

The quartz-syenite hypabyssal sheets

The highly differentiated magmatic rock of the intrusive complex of the Piton des Neiges volcano investigated in this study is a quartz-syenite considered to be the plutonic equivalent of mugearite to benmoreite for the most alkali-rich members. The representative sample is BACH 1, and to a lesser degree RUN 1, the composition of which is reported in Table 2. The differentiated rocks contain ∼10 wt.% $Na_2O + K_2O$ (<4% for host basalt samples RUN 2 and RUN 3), 4–6 wt.% CaO + MgO (16–18% for host basalts), >55 wt.% SiO_2 and a low Ti content. The general petrology of the intrusive rocks of the younger intrusive suite of the Piton des Neiges volcano has been studied previously and the term 'quartz-syenite' has been used to describe the coarse-grained differentiated member (Upton & Wadsworth, 1967). One of the most distinctive petrographic features of the leucocratic quartz-syenite is the relatively coarse-grained texture (grain size >1 mm) compared to that of the intruded volcanic rocks. At hand-sample scale (Fig. 3a), the quartz-syenite of hypabyssal sheets is rather homogeneous both texturally and mineralogically. It consists of a typical interlocked network of euhedral phenocrysts of alkali feldspar with preservation of an exceptionally high intergranular primary macroporosity (pore size may reach >500 µm in diameter) that can be easily identified with the naked eye.

From a mineralogical point of view, these rocks are dominated by feldspar with a strong predominance of alkali feldspar over plagioclase. Under the SEM, the notable scarcity and sometimes the lack of subsolidus replacement texture (perthitic exsolution) in the igneous anorthoclase indicates that the cooling history subsequent to the quartz-syenite sheet emplacement was too rapid to trigger significant subsolidus mineral reactions, thereby preserving the high intergranular porosity that the quartz-syenite was expected to have at the end of its solidification. High intergranular porosity has been found in high-temperature granite issued from newly solidified magma (Sasaki *et al.*, 2003). As a consequence, anorthoclase has a homogeneous chemical composition, as determined by SEM/EDX, ranging from 30% to 40% of orthoclase mole (Or%). Plagioclases are chemically homogeneous with the composition of oligoclase, in which the anorthite mole (An%) ranges from 25% to 30%. In addition to feldspars, the rock mineralogy is completed by small amounts of mafic minerals: Na-rich clinopyroxenes (aegirine augite and aegirine), alkali-rich amphiboles (reibekite-arfvedsonite), magnetite, ilmenite

TABLE 2. Bulk-rock chemical composition (wt.%) of representative samples of basalts (RUN 2 and RUN 3) and small intrusions of highly differentiated magmatic rocks (RUN 1 and BACH 1).

	SiO_2	Al_2O_3	Fe_2O_3	MgO	CaO	Na_2O	K_2O	TiO_2	P_2O_5	LOI	Total
RUN 2	44.10	12.40	12.81	9.56	8.90	2.73	0.11	2.10	0.25	5.73	93.0
RUN 3	46.78	14.16	11.83	6.24	10.04	3.28	0.74	2.39	0.29	2.80	95.8
RUN 1	54.35	16.30	7.55	1.52	3.94	6.16	2.53	1.33	0.43	4.52	94.1
BACH 1	58.12	16.78	6.29	1.04	2.67	6.86	3.17	0.97	0.28	3.16	95.9

LOI = loss on ignition.

https://doi.org/10.1180/clm.2018.51 Published online by Cambridge University Press

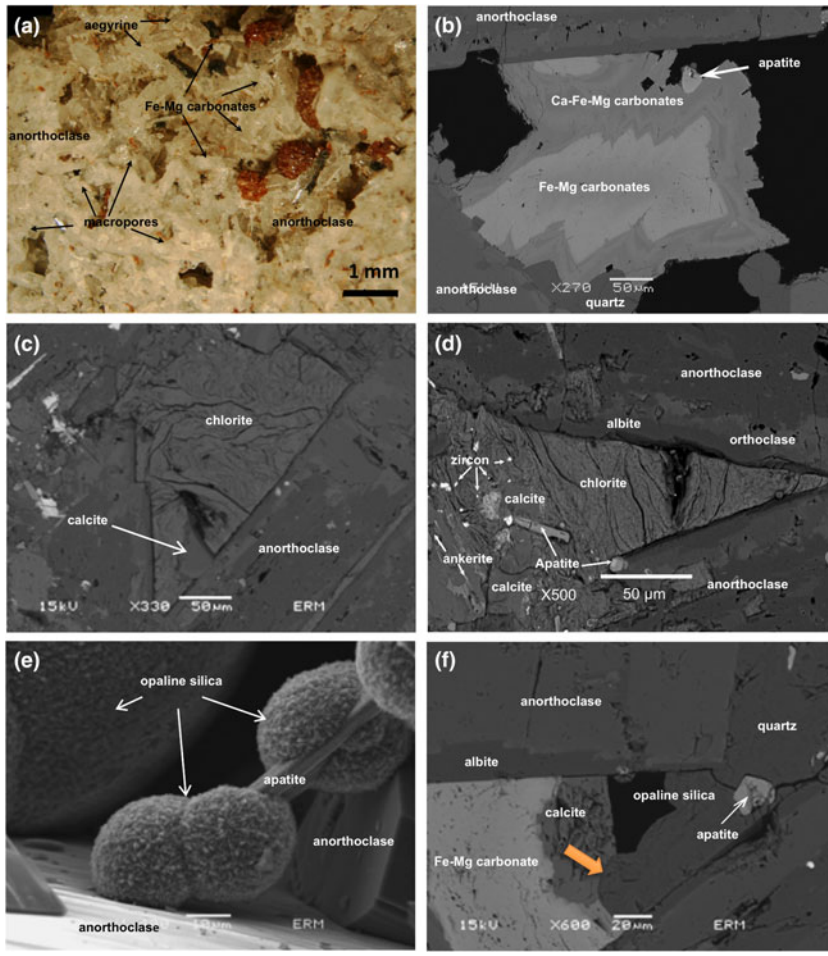

FIG. 3. Petrographic features of the quartz-syenite. (a) Primary macroporosity of the porous quartz-syenite (binocular lens observation of sample BACH 1). (b) Growth of carbonate phenocrysts with zoned composition in the macropores of quartz-syenite in sample BACH 1 (SEM). (c) Infilling in primary macropores by chlorite-like minerals and calcite in sample RUN 8. (d) Cementation of primary pore of quartz-syenite with mineral inclusions of zircon and apatite in sample RUN 11. (e) Lepispheres of opaline silica growing on apatite (SEM, secondary electron observation of sample BACH 1). (f) Details of grain contacts between quartz, carbonates and opaline silica that infilled the primary macroporosity of quartz-syenite in sample BACH 1. The yellow arrow shows the mutual stopping between carbonates and silica.

and subordinate biotite. All of the intrusive rocks are distinctly oversaturated, with the final crystallization of anhedral to subhedral quartz and carbonate phenocrysts often associated with phyllosilicates at the walls of interstitial macropores (*i.e.* at the interstices between the primary feldspar phenocrysts). The phyllosilicates exhibit the optical characteristics of chlorite in thin section (natural greenish colour and low birefringence), and in the absence of a more detailed mineralogical characterization, they will be described hereafter as chlorite-like minerals. From the core to the outer part of the phenocrysts, carbonate crystals display chemical zonation ranging from siderite to ankerite and finally to calcite (Fig. 3b).

Chlorite-like minerals have been observed in all of the studied quartz-syenite samples except for sample BACH 1 (the most highly differentiated term). They occur as cement partially to totally filling the interstitial macropores (Fig. 3c). A very distinctive petrographic feature of these magmatic rocks is the occurrence of chlorite-like

https://doi.org/10.1180/clm.2018.51 Published online by Cambridge University Press

minerals uniquely in the primary macropores, in absence of any alteration features (dissolution and/or secondary crystallization) of primary minerals forming the host quartz-syenite.

A detailed examination of the pore-filling material indicates that quartz, carbonates and all accessory minerals, considered the final mineralogical products of the fractional crystallization of the intrusive mugearitic to benmoreitic magma (*i.e.* zircon, monazite, rutile, apatite, pyrite), are included within the clay cement (Fig. 3d). Spherical aggregates (lepispheres) of opaline silica have been observed as pore-filling materials only in the coarse-grained sample of quartz-syenite (sample BACH 1), which does not present any evidence of clay precipitation (Fig. 3e). In this sample, lepispheres (10–100 µm across) crystallized on the surfaces of all of the primary magmatic minerals, without any trace of dissolution or replacement. The surfaces of the lepispheres consist of aggregates of tiny crystal blades very similar to those reported for opal-CT lepisphere (Graetsch, 1994). The cross-sections of these silica spheres reveal typical colloidal morphology. Several features of growth stopping between quartz, carbonate phenocrysts and the opaline silica lepispheres suggest their syn-crystallization. Indeed, petrographic observations of the crystallization sequence that infilled the primary intergranular porosity indicate that growth of carbonates (ankerite and calcite) was brought to an end by earlier lepidospheres of opaline silica, whose growth was in turn terminated by previously formed quartz and apatite (Fig. 3f).

Basaltic rocks close to the contact with the quartz-syenite hypabyssal sheet

The basaltic rocks adjacent to the differentiated syenitic batholith show typical alteration features (sample BRA 4 in Fig. 2): rare geodic growth of albite and epidote in primary cavities (Fig. 4a) and more systematic presence of clay minerals, sometimes monomineralic chlorite-like minerals, as a replacement for igneous mafic minerals (Fig. 4b). Thus, by contrast with quartz-syenite, the host basaltic material presents all of the features of hydrothermal alteration (*i.e.* strong dissolution of primary feldspars and mafic minerals). Furthermore, zeolite minerals are very common in the hydrothermally altered basaltic lavas of the Piton des Neiges (Upton & Wadsworth, 1967), but are not observed here with chlorite-like minerals in pore infilling.

Quartz, Fe–Mg–Ca carbonates, chlorite-like minerals and pyrite were also observed in brecciated basaltic lava flow (hydraulic breccia) close to their contact with the intrusive quartz-syenite dike (sample RUN 3; Table 1, Fig. 5a). In the breccias, these minerals constitute the cement of the basaltic clasts, which do not present any evidence of alteration (Fig. 5b).

Finally, chlorite-like minerals have also been observed in small spherical ocelli of syenitic composition (several millimetres to 1 cm in diameter) disseminated in the intruded basaltic lava, in association with K-feldspars and rare earth elements bearing epidote and zircon (Fig. 5c,d). These ocelli are generally considered to result from intrusions of differentiated magmatic liquid droplets, enriched in volatiles and incompatible elements in unconsolidated soft basalt. They indicate the presence of liquids of various compositions in the magmatic chamber.

Clay mineralogy

All the XRD patterns obtained from the oriented mounts of particles with sizes <5 µm of the samples containing clay minerals are characteristic of those of

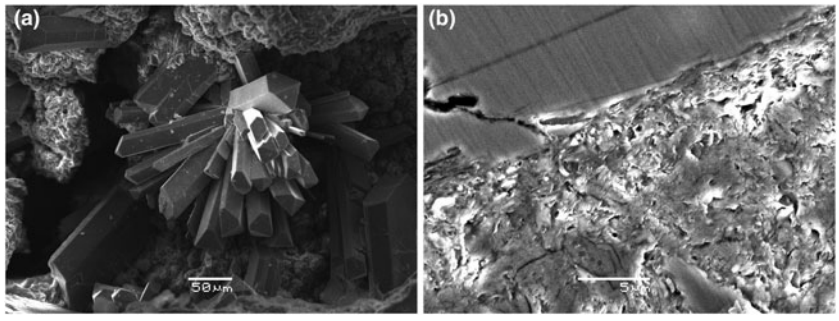

FIG. 4. SEM images of (a) the geodic growth of albite and epidote in the primary cavity of basaltic rocks adjacent to a quartz-syenite sheet and (b) replacement of primary pyroxene by corrensite in sample BRA 4.

https://doi.org/10.1180/clm.2018.51 Published online by Cambridge University Press

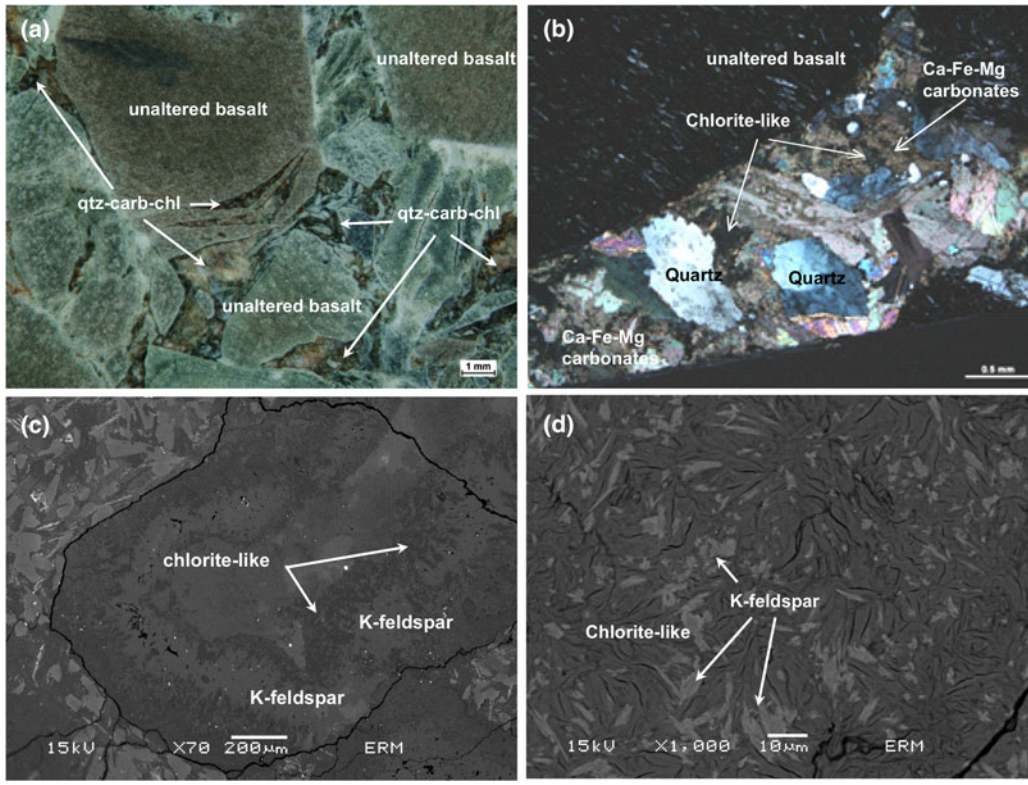

FIG. 5. (a) General aspect of the brecciated basaltic lava close to the contact with a quartz-syenite sheet (binocular microscope). (b) Details of the cementation of the unaltered basalt clasts by coexisting quartz, Ca-Fe-Mg carbonates and chlorite-like minerals (optical microscope, polarized light). (c) Organization of an ocellus. (d) Details of the chlorite-like and K-feldspar association in the ocelli (backscattering electron mode image).

chlorite-smectite (C-S) mixed-layer series (Reynolds, 1980). The observed variations of both the position and profile of the peaks observed for the EG condition (Fig. 6) are indicative of mixed layering with variable amounts of swelling layers among samples.

The XRD traces of sample RUN 14 (Fig. 6a) and BRA 4, which contain the largest amounts of expandable components in the mixed-layer structure, are typical of corrensite (a regularly interstratified chlorite 50%–saponite 50% mixed-layer mineral) with a sharp superstructure reflections at 29 Å (AD) and 31 Å (EG), with eight and nine harmonic reflections in the 2–30°2θ Cu-*K*α range for AD and EG conditions, respectively. The sharpness of these reflections is consistent with the large size of the phyllosilicate flakes observed in thin sections.

The XRD traces of samples RUN 1 and RUN 3 (Fig. 6b), which contain the smallest amounts of expandable components in the mixed-layer structure, are characterized by d00*l* reflections that are close to those of a true chlorite in AD conditions (*i.e.* 14.25, 7.10, 4.73 and 3.54 Å). After EG solvation, the d00*l* reflections expand slightly to 14.42, 7.14 and 4.75 Å and their peak profiles become broader and asymmetric, being typical of a C-S mixed-layer mineral with <10% of an expandable layer. However, in the absence of simulation of the XRD patterns, it is difficult to determine more accurately the structure of this type of C-S mixed layer and more particularly the nature of the expandable component in the mixed-layer structure, which might be smectite or corrensite (Beaufort *et al.*, 1997).

The XRD traces of the clay material present in the other samples of quartz-syenite sheets (RUN 8, RUN 11 and RUN 13) are typical mixtures of corrensite, identified by its superstructure reflections at 29 Å (AD) and 31 Å (EG), and C-S mixed layers rich in chlorite components (Fig. 6c).

https://doi.org/10.1180/clm.2018.51 Published online by Cambridge University Press

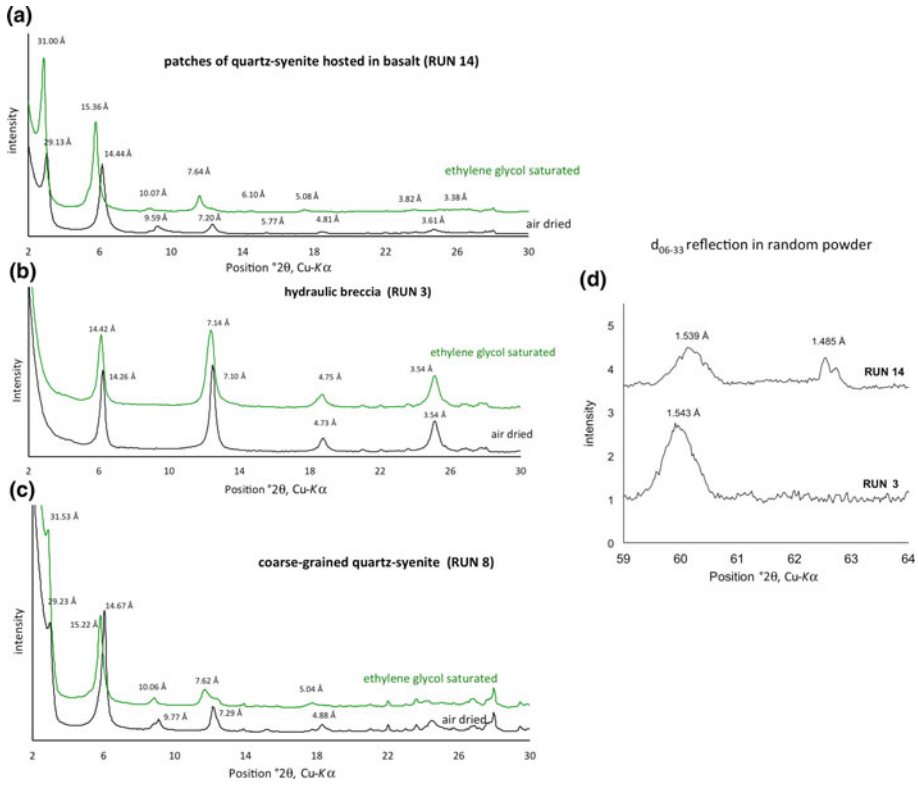

FIG. 6. XRD traces of oriented preparations of the <5 μm fraction acquired in air-dried (black line) and ethylene glycol-saturated (green line) conditions of the quartz-syenite (RUN 14, RUN 8) and the brecciated basalt close to its contact with an intrusive quartz-syenite sheet (RUN 3).

Finally, the d_{06-33} reflection observed near 1.54 Å for samples RUN 3 and RUN 14, which have small and large amounts of expandable components, respectively, confirms the trioctahedral structure of the various members of mixed layers (Fig. 6d).

Under the SEM, the chlorite-like cement is characterized by a very homogeneous distribution of flexuous packets of coarse-grained particles (>2 μm) in the primary macropores of the quartz-syenite, in the absence of alteration of the primary igneous minerals and without evidence of pore lining, zonal distribution or radial orientation of crystallites as are usually observed in hydrothermal alteration or very-low-grade metamorphism of basaltic rocks (Alt, 1999; Schiffman & Day, 1999). The microchemical analyses of clay particles obtained with SEM-EDX are in agreement with the published chemical compositions of corrensite and chlorite-rich C-S mixed layers (Beaufort & Meunier, 1994; Wilson, 2013), corroborating the XRD data. They indicate a significant compositional variation from sample to sample (Table 3), which ranges from nearly pure corrensite (chlorite 50%–smectite 50%) for samples RUN 14 and BRA 4 to a C-S mixed layer very rich in chlorite (chlorite 90%–smectite 10%) for samples RUN 1 and RUN 3 (Fig. 7). No chemical microanalysis of pure chlorite was obtained in the investigated samples, and the chlorite-like particles of the other samples of quartz-syenite (samples RUN 8, RUN 11 and RUN 13) present intermediate chemical compositions between the aforementioned compositional fields (Fig. 7). The chemical variation between samples (Table 3) is marked by a significant increase of iron content of the clay material with increasing chlorite content in the C-S mixed layer. In contrast to the chemical variability between the samples, the low chemical variability within the samples is indicative of the chemical homogeneity of the clay material in each sample.

Isotopic composition

Oxygen isotopic analyses were carried out in the quartz crystals, carbonate and opaline silica in thin

https://doi.org/10.1180/clm.2018.51 Published online by Cambridge University Press

Table 3. Representative EDX microanalyses (oxide wt.%) and structural formulae of chlorite-like minerals formed in quartz-syenite and cement of the brecciated basalt in contact with the quartz-syenite.

	RUN 3	RUN 1	RUN 8	RUN 11	RUN 13	BRA 4	RUN 14
SiO_2	27.47	29.71	30.42	31.20	33.51	35.66	37.05
Al_2O_3	15.59	15.58	14.67	15.07	12.48	12.95	12.55
MgO	10.79	18.87	17.25	13.47	15.99	20.76	20.21
FeO	31.32	20.97	23.73	22.71	21.63	15.29	13.53
TiO_2	0.00	0.06	0.13	0.06	0.06	0.00	0.07
MnO	0.35	0.33	0.13	0.11	0.02	0.16	0.07
CaO	0.15	0.26	0.35	0.66	0.99	1.13	1.01
Na_2O	0.00	0.05	0.12	0.08	0.01	0.01	0.16
K_2O	0.00	0.03	0.00	0.11	0.01	0.11	0.47
Sum	85.67	85.86	86.82	83.47	84.70	86.07	85.12
			Structural formulae based on 14 O atoms				
Si	3.07	3.12	3.20	3.61	3.55	3.58	3.72
Al^{IV}	0.93	0.88	0.80	0.39	0.45	0.42	0.28
Al^{VI}	1.12	1.05	1.02	1.18	1.11	1.12	1.21
Mg	1.80	2.95	2.70	2.09	2.53	3.11	3.03
Fe	2.93	1.84	2.09	2.19	1.92	1.28	1.14
Ti	0.00	0.01	0.01	0.00	0.00	0.00	0.00
Mn	0.03	0.03	0.01	0.02	0.00	0.01	0.01
Ca	0.02	0.03	0.04	0.12	0.11	0.12	0.11
Na	0.00	0.01	0.02	0.01	0.00	0.00	0.03
K	0.00	0.01	0.00	0.00	0.00	0.01	0.06
Oct.	5.88	5.88	5.83	5.48	5.55	5.52	5.38
Int. Ch.	0.04	0.07	0.10	0.24	0.23	0.26	0.31
*X*Fe	0.62	0.38	0.44	0.51	0.43	0.29	0.27

Int. Ch. = interlayer charge; Oct. = octahedral occupancy; *X*Fe = Fe/Fe + Mg.

sections of four samples using SIMS. Carbon isotopic analyses were performed only in carbonate crystals. The analysed samples were quartz-syenitic ocelli (sample BRA 4), medium-grained quartz-syenite hypabyssal sheets (sample RUN 1), non-argilized coarse-grained quartz-syenite hypabyssal sheets (sample BACH 1) and breccia cement at the contact between the intrusive quartz-syenite and basaltic host rock (sample RUN 3). Chlorite-like minerals were not analysed due the lack of reference samples for the correction of the instrumental deviation induced by the ion probe. Several measurements, typically three to seven spots, were performed in each analysed crystal. Examples of spot localization are shown in Fig. 8. Oxygen and carbon isotope compositions are reported in the familiar δ notation relative to the Standard Mean Ocean Water (SMOW) and Pee Dee belemenite (PDB) reference standards, respectively. The low $\delta^{13}C$ values found in the carbonate crystals (0–18‰) associated with $\delta^{18}O$ values ranging from 10‰ to 2‰ (Fig. 9) are indicative of the juvenile origin of the mineralizing fluid (Riley *et al.*, 1999). The $\delta^{18}O$ values in quartz and opal decrease from 14‰ to 9‰ in the coarse-grained syenite and down to 3‰ in the hydraulic breccia. This trend may be indicative of a progressive increase in the water:rock ratio and a progressive contribution of hydrothermal fluid (Holk & Taylor, 2007), with the porous syenite having the greater magmatic signature (*i.e.* >9‰).

DISCUSSION AND CONCLUDING REMARKS

Although the most differentiated terms of the alkaline series do not contain hydrous phyllosilicates in general, the aforementioned petrographic features argue for the occurrence of chlorite-like minerals during the late magmatic activity of the Piton des Neiges volcano. We detail below a possible set of reactions deduced from the petrographic features observed in the quartz-syenite intrusions of the Piton des Neiges edifice.

https://doi.org/10.1180/clm.2018.51 Published online by Cambridge University Press

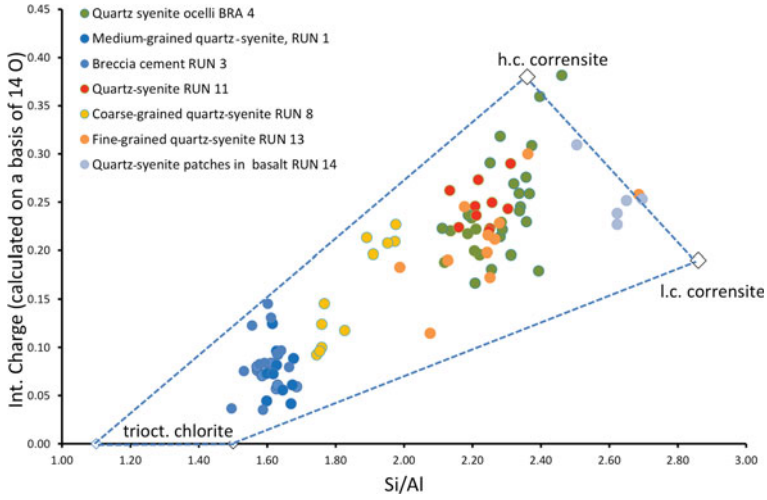

FIG. 7. Si/Al *vs*. interlayer (Int.) charge of chlorite-like minerals related to the late-magmatic activity of the Piton des Neiges volcano. The theoretical compositional fields of trioctahedral (tricot.) chlorite and low-charge (l.c.) to high-charge (h.c.) corrensite have been plotted for reference.

Mineral sequence and fluid origin

The nature of the mineral phases that seal the porous space (*i.e.* carbonates and siliceous phases), their morphology and their composition suggest a late precipitation probably not from a silicate melt, but rather from a CO_2–H_2O fluid. The petrographic relationships of the carbonates and siliceous phases (mutual stopping, isotopic composition) suggest a tardi-magmatic precipitation in the following sequence: apatite/zircon, then quartz/opaline silica and finally carbonates. These phases may be considered as the condensates of a supercritical fluid, while the porous syenitic host rock may be viewed as a reservoir rock. Both transport and precipitation of metals and silicates from such supercritical fluids depend on the

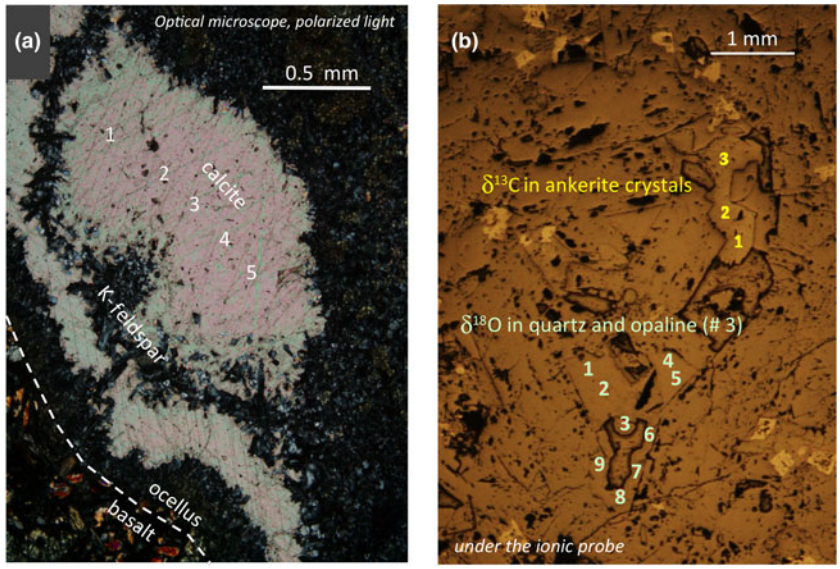

FIG. 8. Example of location of ionic probe analyses. (a) Ocellus of differentiated material in the intruded basalt (optical microscope, sample BRA 4). (b) Coarse-grained syenite (SIMS itself, sample BACH 1).

https://doi.org/10.1180/clm.2018.51 Published online by Cambridge University Press

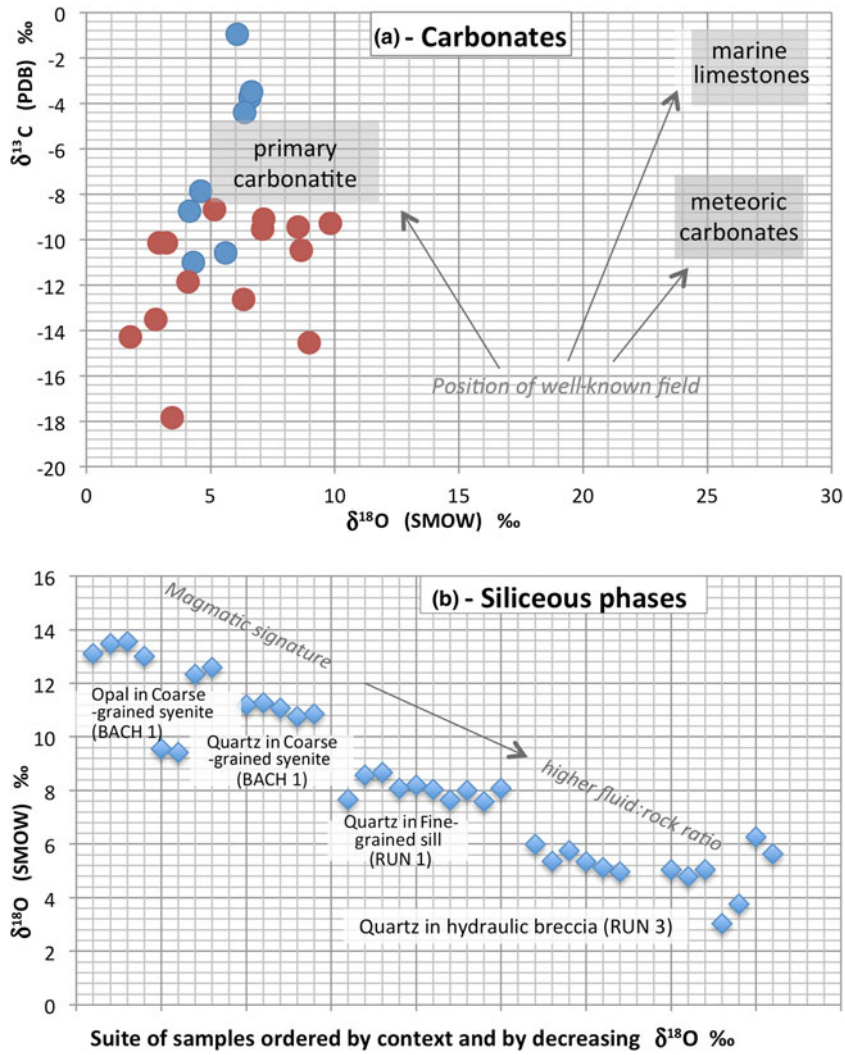

FIG. 9. Diagrams showing the O and C isotopic compositions. (a) Carbon and oxygen isotopic composition of calcite (blue) and ankerite (red) in syenite samples and hydraulic breccia. The samples are not distinguished because all of the isotopic data fall in the field of magmatic carbonates (carbonatite). (b) Oxygen isotopic composition of quartz and opal in various syenite samples and in the hydraulic breccia.

ligands of the fluid. The presence of CO_2 may enhance their mobility or their precipitation (Kokh *et al.*, 2017). The concentration of SiO_2, one of the most mobile silicate constituents, does not exceed a few grams of H_4SiO_4 per kilogram of fluid in high-temperature aqueous fluids under a few or a few tens of megapascals of pressure (Plyasunov, 2011), decreasing considerably with increasing CO_2 content. The amount of the condensed phases, although minor when compared to the reservoir rock, is much greater than that which a supercritical fluid may solubilize in the initial pore volume and requires a larger volume of fluid. However, keeping in mind the magmatic plumbing in cone sheets, and particularly the commonly associated volatile transfer from the magma chamber just after the cone-sheet emplacement and before the annular complex emplacement, it is not necessary to expect an external source of fluid to account for the alteration of the basalt and the pore cementation in the quartz-syenite at sub-magmatic

https://doi.org/10.1180/clm.2018.51 Published online by Cambridge University Press

temperatures. Note that above the second critical point (~700°C, 3.7 GPa; Hermann *et al.*, 2013) there is a continuum between silicate melt and aqueous fluid. However, the predominance of carbonate as a pore filling rather suggests a CO_2-rich fluid, possibly with low density. The system basalt + syenite may be considered as chemically closed, with the exception of volatiles that probably escape to the surface. This assumption requires transfer of a large volume of fluid and can be promoted by a pressure and temperature drop during explosive decompression of the system, as suggested by the presence of hydraulic breccia basalts proximal to the quartz-syenite intrusion.

The petrographic relationships of chlorite-like minerals with carbonates, quartz and accessory minerals, as well as the evidence of direct precipitation (no alteration of the igneous plagioclases or alkali feldspars), suggest crystallization of these clay minerals in continuation of the pore-filling sequence by siliceous phases and carbonates. The rather homogeneous chlorite composition in each sample (Fig. 7) is uncommon in the mixed-layer mineral series that results from low-temperature chloritization (Beaufort *et al.*, 2015, and references therein) and rather suggests a high-temperature system, probably between 700°C (end of the fractional crystallization of the syenite sheet) and 400°C (lower limit of a supercritical fluid).

Significance of corrensite and corrensite-chlorite mixed layers

The high temperatures of late-magmatic stages are not prohibitive of the crystallization of chlorite, but they are less compatible with the crystallization of swelling clay such as the corrensite or corrensite-chlorite mixed layers that form at low to moderate temperatures in a diverse variety of geological environments (Wilson, 2013, and references therein). In subsurface geological environments such as diagenesis, low-grade metamorphism or hydrothermal systems, the occurrence of corrensite is usually related to chloritization (Beaufort *et al.*, 2015, and references therein). Corrensite is generally thought to occur at lower temperatures than chlorite through two major pathways: (1) as a member of a continuous C-S mixed-layer series (Bettison-Varga & Mackinnon, 1997); and (2) as a discrete phase in a discontinuous smectite-corrensite-chlorite sequence (Inoue, 1987; Robinson *et al.*, 2002). The temperature at which corrensite forms in geological systems is poorly constrained, but upper limits of 250–350°C are suggested from several studies of rocks that underwent hydrothermal activity or metamorphism (Kristmannsdottir, 1979; Shau *et al.*, 1990; Barrenechea *et al.*, 2000). At high temperatures, corrensite is often considered as a metastable phase that converts to chlorite depending on kinetic effects (Robinson *et al.*, 2002). Moreover, corrensite has been synthesized hydrothermally by heating oxides for 12–24 h at 500°C and 2 kbar (Roberson *et al.*, 1999), and the formation of expandable chlorite-like minerals during short-term experiments on chlorite hydrothermal synthesis at very high temperatures (up to >800°C) and pressures has been verified (Koizumi & Roy, 1959; Iiyama & Roy, 1963; Fugamalli *et al.*, 2001).

The above considerations suggest that corrensite and other expandable chlorite-like minerals identified in (and close to) the quartz-syenite hypabyssal sheets formed from short-term precipitation processes at very high temperatures (>500°C) during the explosive decompression of the Piton des Neiges volcano. The absence of sub-solidus reactions in igneous Na,K-feldspars and the lack of any typical low-temperature alteration suggest that rock texture and clay minerals formed during the tardi-magmatic phase were preserved in a 'frozen state' after the rapid cooling of the upper part of the dismantled volcano. In such conditions, the variation of expandable-layer contents in the chlorite-like minerals evidenced between the various quartz-syenite hypabyssal sheets may be interpreted as depending on kinetic effects rather than only on temperature. The fluid:rock ratio as well as the mode of fluid transport or the cooling rate might have controlled the rate at which corrensite was formed or was converted to chlorite.

The chemical transfer

The association of Fe,Mg-clays with pore-filling carbonates and siliceous phases may be explained by two coexisting processes. The first is the degassing of exsolved CO_2-rich and SiO_2-rich fluid from the magmatic chamber through the porous syenite sheets, precipitating siliceous and carbonate phases in the primary porosity of the syenite and the fractures of the hydraulic breccia, just after the last stage of crystallization of the silica melt. In this process, the transport of the elements is advective from the chamber towards the surface. However, the chemical composition of the associated clay minerals, and sometimes ankerite, enriched in Fe and Mg, is not in agreement with the expected composition of a fluid generated at the ultimate stage of magmatic differentiation.

https://doi.org/10.1180/clm.2018.51 Published online by Cambridge University Press

The second process corresponds to a centripetal transfer: it suggests the diffusion of Al, Fe and Mg from the intruded basalts towards the primary porosity of the syenite sheet, feeding the crystallization of chlorite-like clays and probably Fe,Mg-carbonate phases. In this model, the diffusive transfer is concurrent with or occurred immediately after the solidification of the syenite sheets and was promoted by the reaction of the intruded basalt with the degassing juvenile fluids. The reaction of the intruded basalt, with a loss of Fe and Mg, may also have contributed to increasing the rate of alterations that basalts have acquired in a previous hydrothermal stage.

This process does not require large volumes of fluids considering the diffusion between two coupled reactions: alteration/remobilization within the intruded basalt *vs*. deposition in the interconnected porosity of the syenite. Such coupled reactions were previously identified in fractured granites with cementation of the fractures by phengite (Berger *et al.*, 1992). In the present study, the factors that led to precipitation of Fe,Mg-clays in the syenite porosity (pH, Eh, a_{SiO2}, temperature) are not clear.

To conclude, the distribution of minerals in space and time was controlled by the porosity of quartz-syenite sheets that constitute a drain for the deep magmatic fluid and by the following crystallization sequence: Na,K-feldspars, aegirine, quartz, zircon, monazite and apatite at the end of melt crystallization, followed by precipitation of opal, sulfides and Ca,Fe,Mg-carbonates from derived magmatic fluid at a subsequent subsolidus stage, and finally chlorite-rich C-S mixed-layer minerals fed by chemical transfer from the intruded basalts (Fig. 10). Although the timing of this sequence is not strictly constrained, the absence of subsolidus reactions and the eruptive context of Réunion Island suggest that this sequence took place early in the cooling sequence of the edifice.

Comparison with calc-alkaline series and application to Mars

The chlorite-rich C-S mixed layers and corrensite encountered in the quartz-syenite hypabyssal sheets of the Piton des Neiges volcano may be viewed as a high-temperature phyllosilicate paragenesis analogue to the dioctahedral micas (muscovite, phengite) often observed in the most differentiated terms (aplite, pegmatite, greisens) of calc-alkaline magmatic series (Fleet, 2003). The remarkable difference between the alkaline and calc-alkaline series is the link between the ascending magma and the root chamber that exists in oceanic volcanism, allowing a large amount of juvenile fluid to transit through the volcanic edifice. Another difference is the proximity of poorly differentiated materials (intruded basalt) as a source of Fe and Mg for

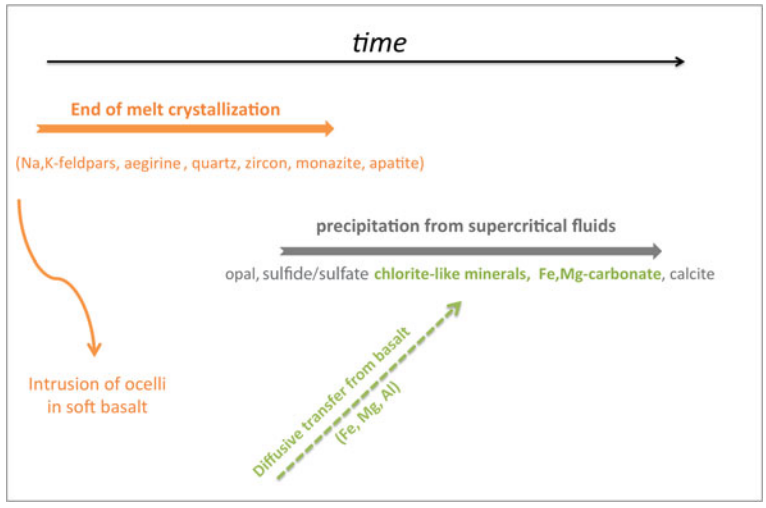

FIG. 10. The crystallization sequence in the studied area. The degassing of exsolved CO_2-rich and SiO_2-rich fluid from the magmatic chamber causes precipitation of siliceous and carbonate phases in the primary porosity of quartz-syenite (grey arrow) just after the last stage of crystallization of the silica melt (yellow arrow). At nearly the same time, or in continuation, the diffusion of Al, Fe and Mg from the intruded basalts altered by the same juvenile fluids feeds the late-magmatic crystallization of chlorite-like minerals (green arrow).

https://doi.org/10.1180/clm.2018.51 Published online by Cambridge University Press

the precipitation of chlorite and corrensite in the syenite. By contrast, the granitic plutons produced by partial melting of continental crust are more easily disconnected from their source.

An important consequence of the late-magmatic activity in the alkaline series is the amount of expandable clay minerals that may be produced by fluid degassing, particularly in the primitive planets when the hydration of the mantle was probably greater than it is today (regarding the terrestrial hydrous Archean komatiites, see *e.g.* Sobolev *et al.*, 2016) and when oceanic volcanism was probably predominant. In the case of Mars, for example, it has been found that the older Noachian terrains contain most of the phyllosilicates detected on the surface (Ehlmann *et al.*, 2013). This is attributed to the weathering of the surface under a clement climate (Bibring *et al.*, 2006), although modelling such warm conditions may be difficult (Forget *et al.*, 2013). However, our knowledge of the mineralogical composition of the surface of Mars is largely based on orbital detection. Meunier *et al.* (2012) demonstrated that a small percentage of tardi-magmatic clays may account for a significant part of the phyllosilicate signal detected by remote sensing techniques. This work has demonstrated how tardi-magmatic clays may form and has shown that a differentiated oceanic crust (mugearite recently observed in the Gale Crater; Stolper *et al.*, 2013) offers all of the conditions for tardi-magmatic clay mineral precipitation, provided that fluids degas for a long time through the porous felsic mass as in a cone-sheet context. Even if weathering or subsurface alteration of basalt is undeniable on Mars, the results of this study indicate that volcanic processes could also contribute to the clay mineralogy of Noachian terrains, as was recently suggested by Cannon *et al.* (2017).

ACKNOWLEDGEMENTS

The authors thank the Laboratoire Géosciences Réunion, Université de La Réunion, for their logistical help in the collection of rock samples. The SIMS analyses were performed in the frame of the National Facilities of the Centre de Recherches Pétrographiques et Géochimiques (Nancy) with the assistance of Claire Rollion-Bard and Michel Champenois.

REFERENCES

Alt J.-C. (1999) Very low grade hydrothermal metamorphism of basaltic igneous rocks. Pp. 169–201 in: *Low-Grade Metamorphism* (M. Frey & D. Robinson, editors). Blackwell Science, Cambridge, UK.

Barrenechea J.F., Rodas M., Frey M., Alonso-Azcarte J., & Mas J.R. (2000) Chlorite, corrensite and chlorite-mica in late Jurassic fluvio-lacrustine sediments of the Cameros Basin northeastern Spain. *Clays and Clay Minerals*, **48**, 256–265.

Beaufort D. & Meunier A. (1994) Saponite, corrensite and chlorite-saponite mixed layers in the Sancerre-Couy deep drill-hole (France). *Clay Minerals*, **29**, 47–61.

Beaufort D., Baronnet A., Lanson B. & Meunier A. (1997) Corrensite: a single phase or a mixed-layer phyllosilicate in the saponite-to-chlorite conversion series? A case study of Sancerre-Couy deep drill hole (France). *American Mineralogist*, **82**, 109–124.

Beaufort D., Rigault C., Billon S., Billault V., Inoue A., Inoue S. & Patrier P. (2015) Chlorite and chloritization processes through mixed layer mineral series in low-temperature geological systems – a review. *Clay Minerals*, **50**, 497–523.

Berger G., Meunier A. & Beaufort D. (2014) Clay minerals formation on Mars: the possible contribution of basalt out-gassing. *Planetary and Space Science*, **95**, 25–32.

Berger G., Turpault M.P. & Meunier A. (1992) Dissolution–precipitation processes induced by hot water in a fractured granite. Part 2: modeling of water rock interaction. *European Journal of Mineralogy*, **4**, 1477–1488.

Bettison-Varga L. & Mackinnon I.D.R. (1997) The role of randomly mixed-layered chlorite/smectite in the transformation of smectite to chlorite. *Clays and Clay Minerals*, **45**, 506–516.

Bibring J.-P., Langevin Y., Mustard J.F. (2006) Global mineralogical and aqueous mars history derived from OMEGA/Mars Express data. *Science*, **312**, 400–404.

Cannon K.M., Parman S.W. & Mustard J.F. (2017) Primordial clays on Mars formed beneath a steam or supercritical atmosphere. *Nature*, **552**, 88–91.

Ehlmann B.L., Berger G., Mangold N., Michalski J.R., Catling D.C., Ruff SW, Chassefiere E., Niles P.B. & Poulet F. (2013) Geochemical consequences of widespread clay mineral formation in Mars' ancient crust. *Space Science Reviews*, **174**, 329–364.

Fleet M.E. (2003) Muscovite and phengite. Pp. 41–286 in: *Rock-Forming Minerals, Vol. 3A, Micas*, 2nd edition. The Geological Society, London, UK.

Forget F., Wordsworth R., Millour E., Madeleine J.-B., Kerber L., Leconte J., Marcq E. & Haberle R.M. (2013) 3D modelling of the early Martian climate under a denser CO_2 atmosphere: temperatures and CO_2 ice clouds. *Icarus*, **222**, 81–99.

Fugamalli P., Stixrude L., Poli S. & Snyder D. (2001) The 10 Å phase: a high-pressure expandable sheet silicate stable during subduction of hydrated lithosphere. *Earth and Planetary Science Letters*, **186**, 125–141.

https://doi.org/10.1180/clm.2018.51 Published online by Cambridge University Press

Graetsch H. (1994) Structural characteristics of opaline and microcrystalline silica minerals. *Reviews in Mineralogy*, **29**, 209–232.

Hermann J., Zhen Y.-F. & Rubarto D. (2013) Deep fluids in subducted continental crust. *Elements*, **9**, 281–287.

Holk G.J., & Taylor H., Jr (2007) $^{18}O/^{16}O$ evidence for contrasting hydrothermal regimes involving magmatic and meteoric–hydrothermal waters at the Valhalla Metamorphic Core Complex, British Columbia. *Economic Geology*, **102**, 1063–1078.

Iiyama J.T. & Roy R. (1963) Unusually stable saponite in the system Na_2O–MgO–Al_2O_3–SiO_2. *Clay Minerals Bulletin*, **5**, 161–171.

Inoue A. (1987) Conversion of smectite to chlorite by hydrothermal and diagenetic alteration, Hokuroku Kuroko mineralization area, northeast Japan. Pp. 158–164 in: *Proceedings of the International Clay Conference, Denver* (L.G. Schultz, H. Van Olphen & F.A. Mumpton, editors). The Clay Minerals Society, Bloomington, IN, USA.

Koizumi M. & Roy R. (1959) Synthetic montmorillonoids with variable exchange capacity. *American Mineralogist*, **44**, 788–805.

Kristmannsdottir H. (1979) Alteration of basaltic rocks by hydrothermal activity at 100-300°C. Pp. 359–367 in: *Proceedings of the International Clay Conference, 1978* (M.M. Mortland & V.C. Farmer, editors). Elsevier, Amsterdam, The Netherlands.

Kokh M.A., Akinfiev N.N., Pokrovski G.S., Salvi S. & Guillaume D. (2017) The role of carbon dioxide in the transport and fractionation of metals by geological fluids. *Geochimica et Cosmochimica Acta*, **197**, 433–466.

Meunier A., Mas A., Beaufort D., Patrier P. & Dudoignon P. (2008) Clay minerals in basalt-hawaiite rocks from Mururoa atoll, French Polynesia. II. Petrography and Geochemistry. *Clays and Clay Minerals*, **56**, 730–750.

Meunier A., Petit S., Ehlmann B.L., Dudoignon P., Westall F., Mas A.El Albani A. & Ferrage E. (2012) Magmatic precipitation as a possible origin of Noachian clays on Mars. *Nature Geoscience*, **5**, 739–743.

Ohtani E. (2005) Water in the mantle. *Elements*, **1**, 25–30.

Plyasunov A.V. (2011) Thermodynamic properties of H_4SiO_4 in the ideal gas state as evaluated from experimental data. *Geochimica et Cosmochimica Acta*, **75**, 3853–3865.

Rançon J.P. (1985) Hydrothermal history of Piton des Neiges volcano (Reunion Island, Indian Ocean). *Journal of Volcanology and Geothermal Research*, **26**, 297–315.

Reynolds R.C. (1980) Interstratified clay minerals. Pp. 249–303 in: *Crystal Structure of Clay Minerals and Their X-Ray Identification* (G.W. Brindley & G. Brown, editors). Mineral Society, London, UK.

Riley T.R., Bailey D.K., Harmer R.E., Liebsch H., Lloyd F. E. & Palmer M.R. (1999) Isotopic and geochemical investigation of a carbonatite-syenite-phonolite diatreme, West Eifel (Germany). *Mineralogical Magazine*, **63**, 615–631.

Roberson H.E., Reynolds R.C. & Jenkins D.M. (1999) Hydrothermal synthesis of corrensite: a study of transformation of the saponite to corrensite. *Clays and Clay Minerals*, **47**, 212–218.

Robinson D., Schmidt S.T. & De Zamora A.S. (2002) Reaction pathways and reaction progress for the smectite-to-chlorite transformation: evidence from hydrothermally altered metabasites. *Journal of Metamorphic Geology*, **20**, 164–174.

Rollion-Bard C., Vigier N. & Spezzaferri S. (2007) *In-situ* measurements of calcium isotopes by ion microprobe in carbonates and application to foraminifera. *Chemical Geology*, **244**, 679–690.

Sasaki M., Fujimoto K., Sawaki T., Tsukamoto H., Kato O., Komatsu R., Doi N. & Sasada M. (2003) Petrographic features of a high-temperature granite just newly solidified magma at the Kakkonda geothermal field, Japan. *Journal of Volcanology and Geothermal Research*, **121**, 257–269.

Sautter V., Fabre C., Forni O. (2014) Igneous mineralogy at Bradbury rise: the first ChemCam campaign. *Journal of Geophysical Research – Planets*, **119**, 30–46.

Sautter V., Toplis M. & Wiens R.C. (2015) *In situ* evidence for continental crust on early Mars. *Nature Geoscience*, **8**, 605–609.

Shau Y.H., Peacor D.R. & Essene E.J. (1990) Corrensite and chlorite/corrensite mixed layers in metabaslts from Northern Taiwan: TEM/AEM, EMPA, XRD and optical studies. *Contributions to Mineralogy and Petrology*, **112**, 119–133.

Schiffman P. & Day H.W. (1999) Petrological methods for the study of very low-grade metabasites. Pp. 108–142 in: *Low-Grade Metamorphism* (M. Frey & D. Robinson, editors). Blackwell Science, Cambridge, UK.

Sobolev A.V., Asafov E.V., Gurenko A.A., Arndt N.T., Batanova V.G., Portnyagin M.V., Garbe-Schönberg D. & Krasheninnikov S.P. (2016) Komatiites reveal a hydrous Archaean deep-mantle reservoir. *Nature*, **531**, 628–632.

Stolper E.M., Baker M.B. & Newcombe M. (2013) The petrochemistry of Jake Matejevic: a Martian mugearite. *Science*, **341**, 1239463.

Upton B.G.J. & Wadsworth W.J. (1965) Geology of Reunion Island, Indian Ocean. *Nature*, **207**, 151–154.

Upton B.G.J. & Wadsworth W.J. (1967) A complex basalt-mugearite sill in Piton des Neiges volcano, Reunion. *American Mineralogist*, **52**, 1475–1492.

Wilson M.J. (2013) Sheet silicates – clay minerals. Pp. 438–443 in: *Rock-Forming Minerals, Vol. 3*. The Geological Society, London, UK.

https://doi.org/10.1180/clm.2018.51 Published online by Cambridge University Press